A Potent Anti-SpuE Antibody Allosterically Inhibits Type III Secretion System and Attenuates Virulence of *Pseudomonas Aeruginosa*

Yang Zhang [1,†], Xiaodan Sun [1,†], Yangyang Qian [2], Hongfei Yi [1], Ke Song [1], Huanhu Zhu [2], Francesco Zonta [1], Weizhong Chen [3], Quanjiang Ji [3], Shane Miersch [4], Sachdev S. Sidhu [1,4,] and Donghui Wu [1]**

1 - Laboratory of Antibody Engineering, *Shanghai Institute for Advanced Immunochemical Studies, ShanghaiTech University, Shanghai, China*
2 - School of Life Science and Technology, *ShanghaiTech University, Shanghai, China*
3 - School of Physical Science and Technology, *ShanghaiTech University, Shanghai, China*
4 - Banting and Best Department of Medical Research, *Terrence Donnelly Center for Cellular and Biomolecular Research, University of Toronto, Toronto, ON, Canada*

Correspondence to Donghui Wu, Sachdev S. Sidhu: *sachdev.sidhu@utoronto.ca, wudh@shanghaitech.edu.cn*
https://doi.org/10.1016/j.jmb.2019.10.026
Edited by Shohei Koide

Abstract

Multidrug-resistant gram-negative bacteria infection is particularly severe within the designated ESKAPE pathogens (*Enterococcus faecium*, *Staphylococcus aureus*, *Klebsiella pneumoniae*, *Acinetobacter baumannii*, *Pseudomonas aeruginosa*, and *Enterobacter* species), which underscores the urgent need to explore alternative therapeutic strategies. The type III secretion system (T3SS) is considered to be a key virulence factor in many gram-negative bacteria, and T3SS is in turn regulated by SpuE in *P. aeruginosa*, which is a spermidine binding protein from an ATP-binding cassette transporter family and highly conserved within ESKAPE pathogens. Here, we identified a potent anti-SpuE antagonistic antibody that allosterically inhibits the expression of T3SS and attenuates virulence of *P. aeruginosa*. X-ray crystallography and molecular dynamics simulations revealed that binding of antibody to SpuE induces a change in the dynamics of SpuE, which in turn may reduce spermidine uptake by *P. aeruginosa*. The antibody could serve as a template for developing novel biologics to target a broad spectrum of gram-negative bacteria.

Introduction

In recent decades, multidrug resistance bacteria have become a global threat to public health. This situation is particularly severe within the designated ESKAPE pathogens, which include *Enterococcus faecium*, *Staphylococcus aureus*, *Klebsiella pneumoniae*, *Acinetobacter baumannii*, *Pseudomonas aeruginosa*, and *Enterobacter* species [1]. Most clinically approved antibiotics act by either killing bacteria or by slowing their growth [2]. Ironically, the killing mechanism may drive bacteria to rapidly evolve antibiotics resistance to survive [2]. Thus, there is an urgent need for alternative strategies to control bacterial infection, and targeting of bacterial virulence factors may be one such option.

The type III secretion system (T3SS) is a major virulence factor in many gram-negative bacteria including *Shigella*, *Salmonella, Chlamydia*, *Yersinia*, *Escherichia,* and *Pseudomonas* species [3,4]. Expression of T3SS is strongly correlated with poor clinical outcomes and inactivation or downregulation of T3SS genes significantly attenuates bacterial virulence [5–7]. Thus, targeting T3SS is quite appealing in that it does not kill bacteria but can attenuate virulence and enable clearance by the host immune system [8].

P. aeruginosa is an opportunistic human pathogen, which can cause severe acute and chronic infections in patients with compromised immunity [9]. The *P. aeruginosa* T3SS is a needle-like structure encoded by more than 40 genes, most of which are

clustered in a 12-kilobase region of the genome [8]. The T3SS locus consists of coordinately regulated and functionally clustered genes encoding proteins responsible for regulation (*exs* genes), secretion (*pcr* and *pop* genes) and translocation (*pcr* and *pop* genes) of T3SS [8], whereas genes encoding virulent effector proteins (*exo* genes) are located separately [10]. Thus far, four toxic effectors have been identified. ExoS and ExoT possess GTPase-activating protein activity and ADP-ribosyltransferase activity, which disturb the host cell actin cytoskeleton and promote cell death [11]. ExoU possesses phospholipase A_2 activity, which results in cellular membrane damage [12], and ExoY is an adenylate cyclase that impairs cell proliferation by causing disassembly of microtubules [13,14].

ExsA, a master regulator of T3SS, is under the control of the *exsCEBA* promoter [15]. Knockout of the *SpuEFGH* operon or *SpuE* alone has been shown to dramatically repress the activity of the *exsCEBA* promoter, and consequently, to attenuate the cytotoxicity of *P. aeruginosa* by downregulating the expression of most T3SS genes [16]. SpuEFGH belongs to the ATP-binding cassette (ABC) transporter family for uptake of spermidine and other polyamines, in which SpuE is a periplasmic spermidine binding protein, SpuG and SpuH constitute the transmembrane channel, and SpuF is a cytoplasmic ATPase [16–18].

Given its role in regulating the *exsCEBA* promoter, inhibiting spermidine transport through SpuEFGH could attenuate T3SS virulence and could thus have therapeutic potential for treating *P. aeruginosa* infection. In agreement with this hypothesis, a polyamine inhibitor that mimicked spermidine reduced bacterial burden and protected mice from lethal *P. aeruginosa* infection [19]. Moreover, an antibody that binds spermidine and spermine has been shown to provide significant protection in a murine model of acute *P. aeruginosa* infection [20]. However, spermidine, spermine and other polyamines are widely distributed and play important roles in multicellular organisms, including regulation of cell growth, proliferation, and protein translation [21–23]. Consequently, while targeting spermidine may have efficacy against *P. aeruginosa* infection, it could also have unforeseen adverse effects in humans [20]. Therefore, developing antibodies that directly target SpuE may maximize the therapeutic potential while minimizing possible side effects.

Here, we explored the concept of using antibodies that target SpuE to prevent spermidine transport, and consequently, to inhibit T33S assembly and *P. aeruginosa* infection. We used phage display to derive an anti-SpuE single-chain variable fragment (scFv5) that attenuated T3SS-mediated cytotoxicity of *P. aeruginosa* in human epithelial cells. We found that scFv5 significantly improved survival of the nematode *Caenorhabditis elegans* challenged by *P. aeruginosa* infection. The SpuE structure consists of two globular domains linked by a hinge and spermidine binding induces an open-to-closed conformational switch of the two domains around the hinge [17]. The crystal structure of scFv5 in complex with SpuE-spermidine showed that the antibody bound the hinge region and molecular dynamics simulations implied that the binding of scFv5 forced SpuE into a less closed conformation that may subsequently weaken spermidine binding and release. Thus, scFv5 could serve as a template for the design of novel biologics to treat *P. aeruginosa* infection by attenuating spermidine transport and T3SS function.

Results

Isolation and characterization of anti-SpuE scFvs

We used a naïve phage-displayed library of human scFvs [24] to select for antibodies that could recognize spermidine-bound SpuE. After three rounds of binding selections, single clones were analyzed by phage ELISA, and clones that bound specifically to SpuE-spermidine were subjected to DNA sequencing to decode sequences of displayed scFvs. This analysis revealed three scFvs with unique complementarity-determining region (CDR) sequences (Fig. 1A and Supplementary Fig. 1). The three scFvs were purified as free proteins by recombinant expression in bacteria, and binding to SpuE-spermidine was assessed by enzyme-linked immunosorbent assay (ELISA). All three scFvs bound to the antigen, and in particular, scFv5 showed the highest apparent affinities by both direct binding ELISA (Fig. 1B, $EC_{50} = 1.6$ nM) and competition ELISA (Fig. 1C, $IC_{50} = 16.7$ nM).

We also used competition ELISAs in epitope binning experiments to determine whether each scFv could block binding of different scFv-phage. Immobilized SpuE was first treated with a saturating concentration of a particular scFv, and subsequently, binding of scFv-phage was assessed by phage ELISA. This assay showed that each of the three scFv proteins was able to block binding of all three scFv-phages, suggesting that the three scFvs bind to overlapping epitopes or are able to induce conformational changes that prevent binding of other scFvs (Fig. 1D).

Effects of scFv5 on the expression of T3SS proteins *in vitro*

Given its high affinity for SpuE, we chose scFv5 for further studies. To assess effects of the antibody on SpuE in the periplasm *P. aeruginosa*, we purified a

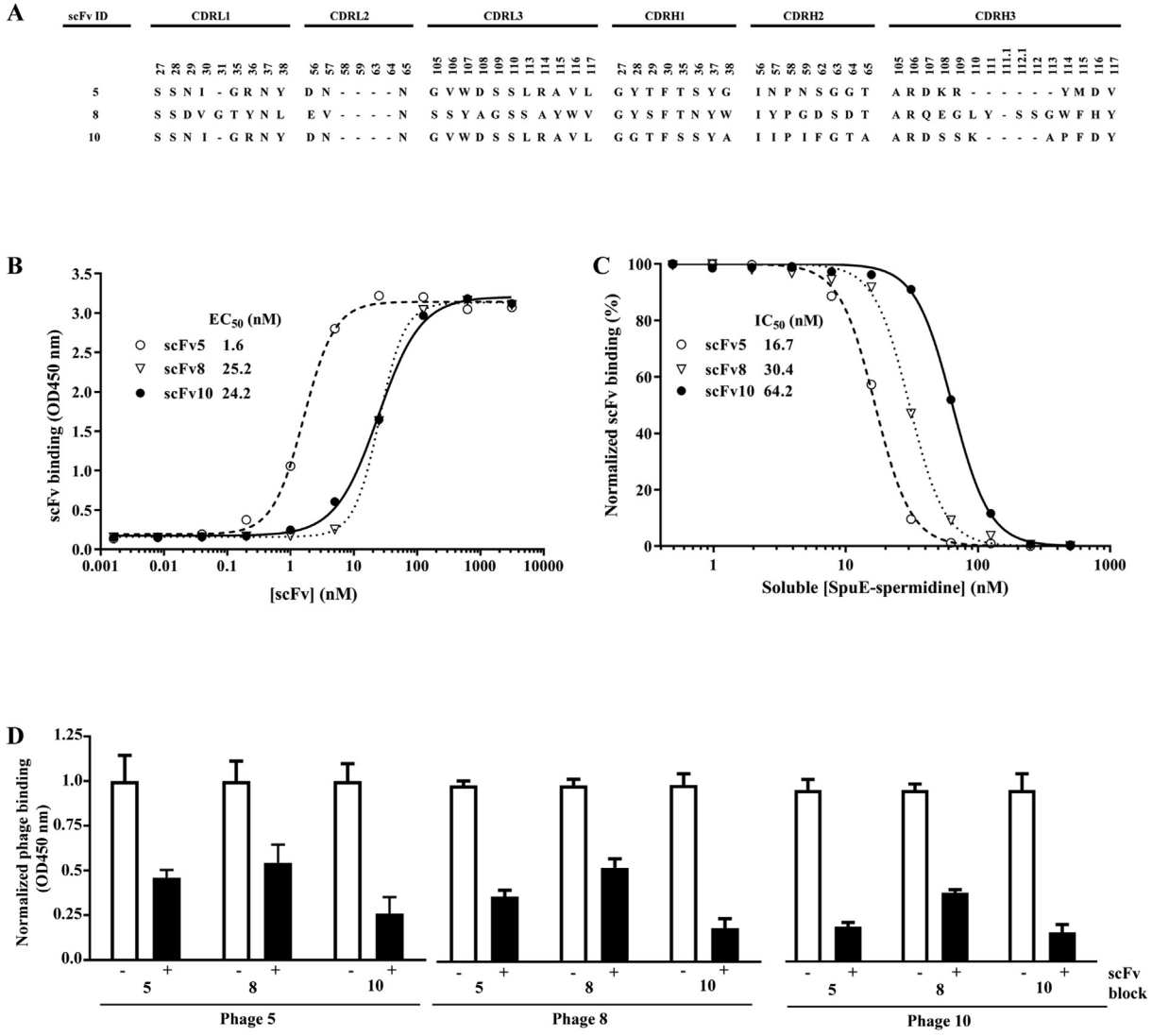

Fig. 1. - Anti-SpuE antibody sequences and binding characteristics. (**A**) The sequences of the CDRs are numbered according to IMGT standards. (**B**) Dose response curves for ELISAs detecting serial dilutions of scFv protein (x-axis) binding to immobilized SpuE-spermidine (y-axis). (**C**) Dose response curves for competitive ELISAs detecting binding of scFv protein to immobilized SpuE-spermidine (y-axis) in the presence of serial dilutions of solution-phase SpuE-spermidine (x-axis). (**D**) To assess relative epitopes, scFv-phage binding to immobilized SpuE-spermidine was measured by phage ELISA (white bars) and compared with binding in the presence of saturating scFv protein (black bars). Error bars represent standard deviation of three independent experiments.

fusion protein consisting of scFv5, followed by a linker (sequence: AGAGAGAGAGAGAGAGAS), followed by a membrane-penetrating peptide (MPP, sequence: KRKKRKKRK) that destabilizes bacterial cell membranes and enables fused protein to traverse the outer membrane [25]. The fusion protein (scFv5-MPP) was tested for effects on T3SS in *P. aeruginosa*.

ExoS, a key effector protein secreted by T3SS and translocated into eukaryotic cells, elicits a host cytotoxic response through its ADP-ribosyltransferase activity [26]. To assess whether scFv5-MPP could inhibit the secretion of ExoS *in vitro*, wild-type (WT) *P. aeruginosa* strain PAO1 was treated with scFv5-MPP, and ExoS present in the culture supernatant was detected by Western blotting (Fig. 2A). Consistent with a previous report [16], secretion of ExoS was almost completely abrogated in a *P. aeruginosa* PAO1 derivative strain with a deletion of *spuE* (Δ*spuE*). Treatment with scFv5-MPP also reduced ExoS secretion in a dose-dependent manner, whereas no effect was observed for a negative control scFv (Supplementary Fig. 1) fused to the membrane-penetrating peptide (scFv-MPP).

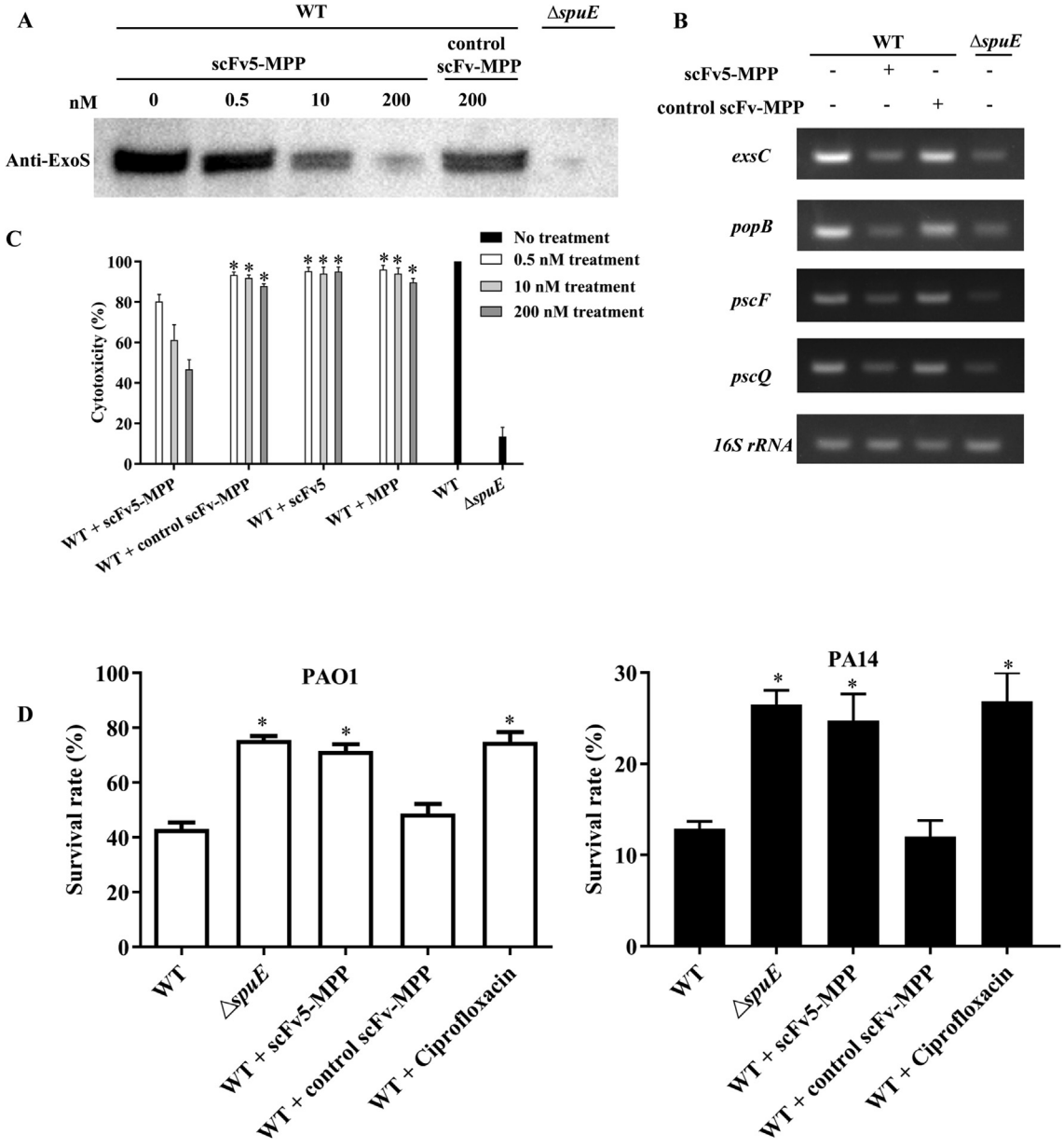

Fig. 2. - ScFv5-MPP downregulates *P. aeruginosa* T3SS and attenuates *P. aeruginosa* toxicity in cells and animals. WT refers to *P. aeruginosa* wild type; Δ*spuE* refers to *spuE* gene knock out of *P. aeruginosa*. (**A**) Western blot showed that scFv5-MPP inhibited ExoS secretion by *P. aeruginosa* PAO1 in a dose-dependent manner. (**B**) RT-PCR analysis showed that scFv5-MPP treatment downregulated transcription of four T3SS genes from different operons in *P. aeruginosa* PAO1. Data shown are one representative of three independent repeats. (**C**) scFv5-MPP reduced cytotoxicity of *P. aeruginosa* to A549 epithelial cells in a dose-dependent manner. Statistical analysis was conducted by comparing scFv5-MPP-treated group with other treatment groups at each corresponding concentration. Asterisk refers to the P value less than 0.02. (**D**) Killing assay of *C. elegans* by *P. aeruginosa* PAO1 (white bars) and PA14 (black bars). Statistical analysis was conducted by comparing the survival rate of *C. elegans* infected with *P. aeruginosa* WT with that from other groups. Asterisk refers to the P value less than 0.02.

To evaluate the effect of scFv5-MPP on regulation of T3SS gene expression, reverse transcription polymerase chain reaction (RT-PCR) was used to quantitate the transcription of four representative genes, *exsC*, *popB*, *pscF*, and *pscQ*, located in four distinct operons of T3SS. In WT *P. aeruginosa* PAO1, treatment with scFv5-MPP reduced expression of all four genes whereas the negative control scFv-MPP had no effect (Fig. 2B). As expected, gene expression was also reduced in *P. aeruginosa*

Δ*spuE*. Taken together, these results show that scFv5-MPP inhibits T3SS in *P. aeruginosa* cells.

Effects of scFv5-MPP on *P. aeruginosa* toxicity in cells and animals

We assessed the ability of scFv5-MPP to inhibit the cytotoxic effects of *P. aeruginosa* in the human epithelial cell line A549 (Fig. 2C). As expected, *P. aeruginosa* Δ*spuE* showed significantly decreased cytotoxicity in A549 cells compared with WT *P. aeruginosa* PAO1, confirming that *spuE* is required for T3SS-mediated cytotoxicity. Treatment of WT *P. aeruginosa* PAO1 with scFv5-MPP reduced cytotoxicity in A549 cells in a dose-dependent manner, whereas treatment with control scFv-MPP, scFv5 or MPP had no effect. Taken together, these results show that scFv5 inhibits SpuE in *P. aeruginosa* cells, provided that delivery into the periplasm is facilitated by an MPP fusion, and consequently, scFv5-MPP inhibits T3SS-mediated cyotoxicity in A549 cells.

We used a well-established *C. elegans* animal gut infection model [27] to study the protective effect of scFv5-MPP against *P. aeruginosa* infection. As expected, the survival rate of *C. elegans* that were infected with WT *P. aeruginosa* PAO1 was significantly lower than that of *C. elegans* infected with *P. aeruginosa* Δ*spuE* (Fig. 2D, left), confirming the positive role for *spuE* in regulating the virulence of *P. aeruginosa*. Preincubation of *P. aeruginosa* PAO1 with scFv5-MPP before treatment of *C. elegans* significantly increased the survival rate of *C. elegans* to levels comparable to treatment with *P. aeruginosa* Δ*spuE*, whereas treatment with the negative control scFv-MPP did not significantly improve the survival rate. Moreover, the survival benefit conferred by scFv5-MPP treatment was similar to that conferred by treatment with the antibiotic Ciprofloxacin as a positive control [25]. Similar results were obtained with the *P. aeruginosa* strain PA14 (Fig. 2D, right), which is more virulent than PAO1 [28]. Taken together, these results showed that scFv5-MPP is efficacious for protecting *C. elegans* from *P. aeruginosa* toxicity.

Structure of scFv5 in complex with SpuE-spermidine

To study the molecular basis for the effects of scFv5 on SpuE function, we crystallized scFv5 bound to SpuE-spermidine and solved the complex structure by molecular replacement. Data collection and refinement statistics are shown in Supplementary Table 1. The crystal belonged to $P2_1$ space group and one asymmetric unit (ASU) contained 18 copies of complex. The averaged total buried interface within the 18 copies was 1700 ± 57 Å^2 and was equally contributed by SpuE and scFv5. One copy of the complex (chain A, SpuE-spermidine; chain a, scFv5) was used to illustrate the overall structure and the interface of the complex.

ScFv5 interacts with the hinge region that connects the two domains of SpuE, and the heavy-chain variable (VH) and light-chain variable (VL) domains contribute 402 and 451 Å^2 of buried surface area, respectively (Fig. 3A). The three light-chain CDRs and heavy-chain CDRH3 make polar interactions that appear to stabilize the hinge region (Fig. 3B). In CDRL1, the main chains of Arg36^L and Tyr38^L form hydrogen bonds with the main chains of Glu328 and Asp326, respectively, and the Tyr38^L side chain forms a hydrogen bond with the main chain carboxyl of Tyr331. In CDRs L2 and L3, the side chains of Asn57^L and Arg114^L form a hydrogen bond or a salt bridge with the side chains of Glu328 or Asp321, respectively. In CDRH3, the side chains of Asp107^H and Arg109^H form a salt bridge or a hydrogen bond with the side chain of Lys322 or Asp326, respectively.

Effects of scFv5 on the kinetics and dynamics of SpuE towards spermidine

It is known that B factors from X-ray crystallographic data can be used to study protein dynamics [29]. Interestingly, based on B factor analysis of SpuE, manual examination of spermidine density and superposition to SpuE-spermidine (PDB code: 3ttn_A), the 18 copies in the asymmetric unit can be clustered into two distinct groups. Group 1 comprises 12 copies of complex, which are characterized by averaged low B factor (50.0 Å^2), well-resolved spermidine electron density and low averaged root-mean-square deviation (RMSD) (0.4 Å) (Fig. 4, left). Group 2 comprises the other 6 copies of complex, which are characterized by averaged high B factor (75.6 Å^2), poorly resolved spermidine electron density and high averaged RMSD (0.6) (Fig. 4, right). These differences in the two groups imply that binding of scFv5 may weaken the binding of SpuE to spermidine.

Isothermal titration calorimetry (ITC) was used to analyze the effect of scFv5 on the binding of SpuE to spermidine. As shown in Fig. 5, the dissociation constant (K_D) of SpuE to spermidine was 2.7 nM. In contrast, the K_D of SpuE to spermidine was weakened to 29.8 nM in the presence of scFv5. This led to a net Gibbs free energy (ΔG) loss of around 1.4 kcal/mol from −11.7 kcal/mol in the absence of scFv5 to −10.3 kcal/mol in the presence of scFv5, which was partitioned into the dominant net TΔS entropic loss of around 2.0 kcal/mol and the net ΔH enthalpic gain of around 0.6 kcal/mol. It is known

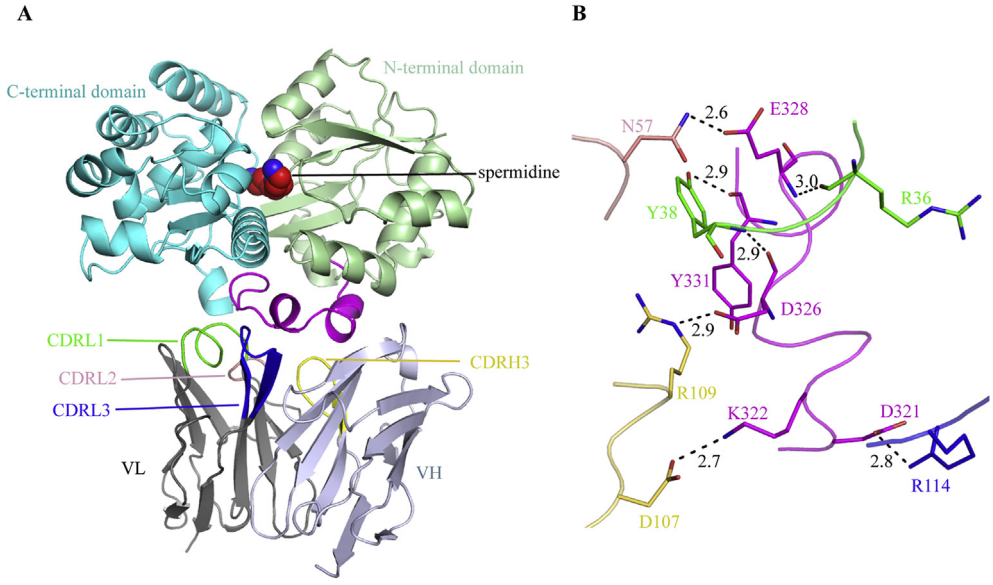

Fig. 3. - The crystal structure of SpuE-spermidine in complex with scFv5. (**A**) Overall structure of the scFv5-SpuE-spermidine complex. SpuE is colored as follows: N-terminal domain (pale green), hinge (magenta), C-terminal domain (cyan). Spermidine atoms are shown as spheres colored as follows: carbon (red), nitrogen (blue). The scFv5 VL and VH domains are colored grey and light blue, respectively, and the CDRs are colored as follows: CDRL1 (green), CDRL2 (salmon), CDRL3 (blue) and CDRH3 (yellow). (B) Interactions between scFv5 CDRs and the SpuE hinge region, colored as in panel A. Dashed lines represent hydrogen bonds or salt bridges with the measured distance shown in Angstroms.

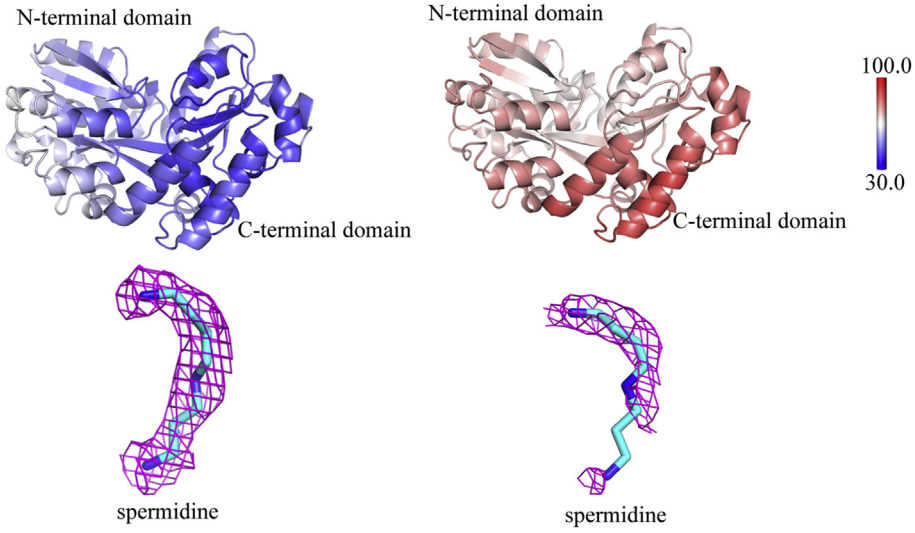

Fig. 4. - B factor profile and spermidine electron density of the 18 copies within the asymmetric unit of crystal lattice are divided into two groups. Left: the group with an averaged low B factor and well-resolved spermidine electron density; right: the group with an averaged high B factor and poor-resolved spermidine density. Upper panel is for B factor distribution based on overall structure; lower panel is for spermidine electron density map 2mFo-DFc contoured at 1.0 σ. B factor color scale is shown in a bar ranging from 30.0 to 100.0 $Å^2$.

that ΔS reflects the dynamics and flexibility of the system and one main part of ΔS in protein-ligand binding is contributed by solvent effects [30]. Clearly, binding of spermidine to SpuE is both enthalpically and entropically favorable. Moreover, crystal structures showed that SpuE undergoes an open-to-closed conformational change on spermidine binding [17]. The favorable entropy change on

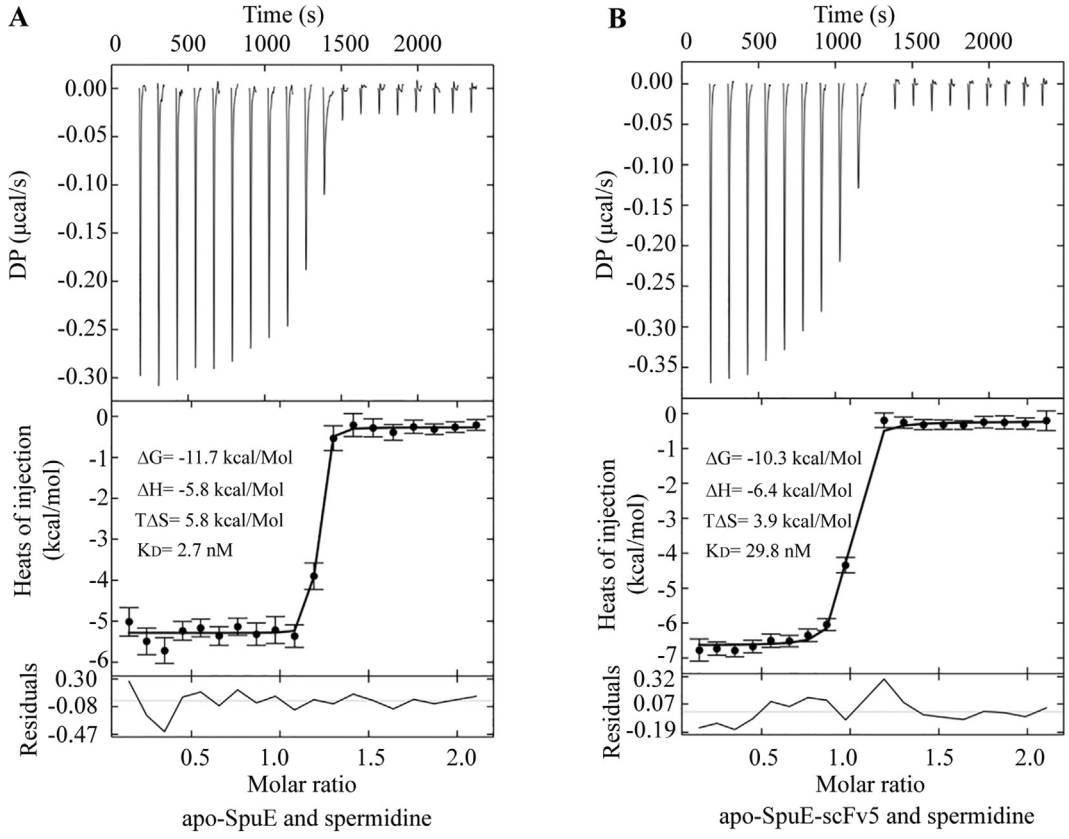

Fig. 5. - Thermodynamic characterization of the interaction of apo-SpuE with spermidine in the presence or absence of scFv5. Isothermal titration calorimetry of (**A**) apo-SpuE and (**B**) apo-SpuE-scFv5 binding to spermidine at 25 °C. The top panel shows the thermogram provided by NITPIC, the middle panel and bottom panel analyzed using SEDPHAT one-site binding model show the isotherm and residuals, respectively.

spermidine binding may be achieved by releasing the constrained interfacial water molecules within the open SpuE interdomain surface into the bulk solvent on formation of the closed SpuE. Though spermidine binding to SpuE-scFv5 complex is also enthalpically and entropically favorable, the entropic positive change is less (3.9 kcal/mol) as compared with that of spermidine binding to SpuE (5.8 kcal/mol), implying SpuE may be partially closed in the presence of scFv5 on spermidine binding and coupled with less constrained water release. However, it has to be pointed out that entropy consists of multiple types in protein-ligand interactions including solvent entropy, protein conformational entropy, ligand conformational entropy, rotation-translational entropy and other unidentified entropy [30,31]. Accurate measurement of each type of entropy contribution is challenging [31].

Although a structure of the SpuEFGH spermidine importer is not available, comparison of SpuE in the spermidine-bound state to ModA in the molybdate-bound state by Dali analysis [32] showed a Z score of 16.4 between the two structures, suggesting that the overall folds of the SBPs are similar and that both importers may use a similar transmembrane pathway for ligand uptake. We thus used the molybdate ABC transporter $ModAB_2C_2$ in the pretranslocation state, a state that the ligand-bound SBP in a closed conformation starts to make initial contact with transmembrane channels [33], to model the corresponding state of spermidine import by SpuEFGH. SpuE in the spermidine-bound state was superposed to ModA in the molybdate-bound state. Both domains of ModA are involved in recognition of ModB transmembrane channels (Fig. 6A, purple regions), and when SpuE was superposed to ModA, the interaction regions from ModA corresponded to the regions encompassing residues 53–71 in the N-terminal domain and residues 215–232 in the C-terminal domain of SpuE (Fig. 6B, purple regions). A 200 ns-scale molecular dynamics simulation was then performed to monitor the relative distances between the mass centers of the corresponding regions of SpuE from three different structures (Fig. 6C). For the spermidine-bound SpuE alone, the relative distance between these regions was

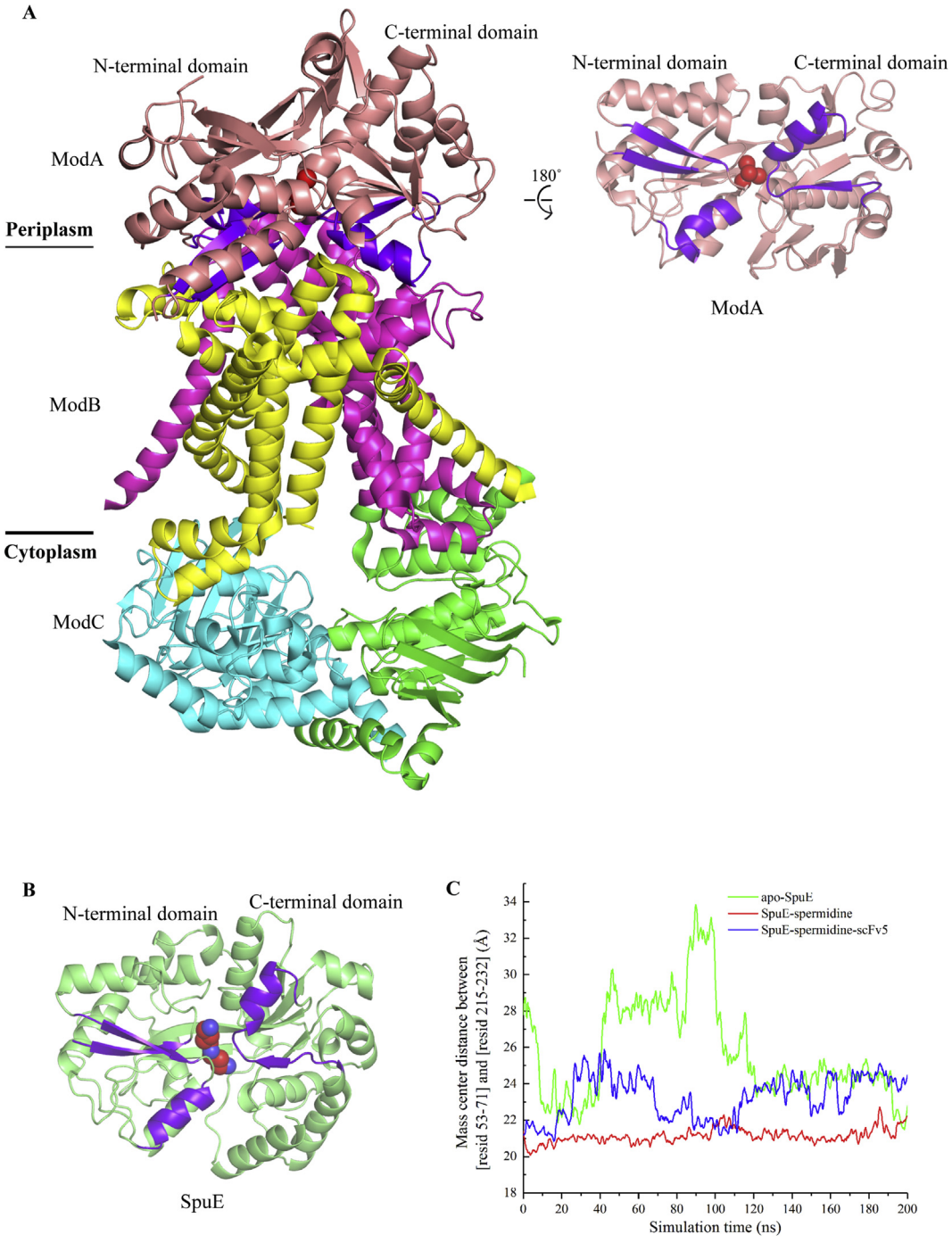

Fig. 6. - Effect of scFv5 on the dynamics of SpuE towards spermidine uptake. Crystal structure of Molybdate $ModAB_2C_2$ ABC importer (PDB code: 2ONK) (**A**) was used to model spermidine importer. (**B**) SpuE was shown in the same orientation as that in ModA. Color schemes: ModA in salmon; ModB homodimeric transmembrane channels in yellow and magenta, respectively; ModC homodimeric ATPase in green and cyan, respectively; SpuE in pale green; the interaction regions in ModA and the corresponding regions in SpuE to the transmembrane channels from both the N-terminal and C-terminal domains in purple blue; molybdate and spermidine in sphere with nitrogen in blue and other atoms in red. (C) The mass center distance between the interaction regions from both domains in SpuE was analyzed for apo-SpuE (PDB code: 3TTL), SpuE-spermidine complex (PDB code: 3TTN), and SpuE-spermidine-scFv complex (PDB code: 6KIM) over a 200 ns-scale molecular dynamics simulation.

within a narrow range of 20−22 Å in the whole 200 ns simulation, and this narrow range may be essential for spermidine-bound SpuE to efficiently dock with the transmembrane channels to initiate spermidine uptake. In contrast, the relative distance between these regions for the apo-SpuE fluctuated significantly within a wide range of 22−34 Å, reflecting that SpuE was quite dynamic in the absence of spermidine. Interestingly, in the presence of scFv5, the relative distance between these regions increased and ranged from 21 to 26 Å, as compared with the narrow range of 20−22 Å for the spermidine-bound SpuE alone, implying that scFv5 binding can induce the closed SpuE-spermidine complex to adapt a less closed conformation that may perturb the subsequent docking of spermidine-bound SpuE with the transmembrane channels. To be noted, the observed dynamics pattern for both apo-SpuE and spermidine-bound SpuE is similar to a previous paramagnetic nuclear magnetic resonance study of maltose-binding protein in the presence or in the absence of maltose [34], highlighting molecular dynamics simulation can become a complementing research tool to study protein dynamics [35].

Discussion

ABC importers of various nutrients including sugars, amino acids, peptides, polyamines, metal ions, sulfate are indispensable for support of bacterial growth and virulence [36]. Thus components of ABC importers in bacteria are appealing targets for antibody and vaccine development [37]. SpuE is one such component, closely involved in the regulation of T3SS expression and virulence in *P. aeruginosa* [16,18].

A survey of many structures of solute-binding proteins (SBPs) from ABC importers in bacteria reveals that most SBPs are composed of two globular domains connected by a flexible hinge, and that substrate binding induces an open to closed conformational switch of SBPs around the hinge region [38]. Structures of several antibodies bound to SBPs of bacterial ABC importers have revealed two distinct epitopes. For an epitope on MntC in *S. aureus*, which is responsible for Mn(II) binding, it was proposed that antibody binding may sterically perturb interactions with the transmembrane protein MntB [39]. For a different epitope on BtuF in *Escherichia coli*, which is responsible for uptake of vitamin B12, it was shown that a single-domain antibody targeted the cleft between the N- and C-terminal domains, and in so doing, blocked substrate binding and interactions with the transmembrane protein BtuC [40]. Another single-domain antibody, which bound to maltose binding protein of *E. coli* and also targeted the substrate binding cleft, acted through a mechanism similar to that of the anti-BtuF antibody [41].

In contrast to previous reports of antibodies that inhibit ligand transport through steric blockage, we identified an antibody that targets the hinge of SpuE and thus inhibits spermidine transport through an allosteric mechanism. Of note, we identified the SpuE hinge epitope from a naïve human antibody library, implying that the hinge region from SpuE is prone to be recognized by natural human B cell receptors and may be used as a vaccine candidate. Moreover, given that the flexible hinge is well conserved in many bacterial ABC importers, combination of all known bacterial ABC importer hinge regions for vaccine development may produce prophylactic effect against many bacterial pathogens.

Unlike gram-positive bacteria, gram-negative bacteria have an impermeable outer membrane barrier that makes many potentially therapeutic macromolecules ineffective because of a lack of access to their targets. Pioneering studies showed that fusion of endolysin with MPP can effectively facilitate endolysin to cross the barrier to degrade the peptidoglycan layer within the periplasm [42]. MPP functions by disturbing the negatively charged lipopolysaccharides, a major component of gram-negative bacterial outer membrane [42]. Here, we showed that the efficacy of scFv5 to target SpuE within the periplasm requires its fusion with MPP. However, it should be noted that MPP may cause disturbance to human normal cell membranes, although a previous study suggested that MPP appears to be safe as it cannot lyse human red blood cells or B cells [43]. Further study will be needed to assess the biodistribution and toxicity of scFv5-MPP.

The innate immunity between *C. elegans* and mammalian models is well conserved [44]. Moreover, the advantages of using *C. elegans* as a model host to study the virulence of human and animal microbial pathogens are its facile and economical [44,45]. However, we have to point out that eradication of microbial pathogens by host requires both innate and acquired immunities, and thus, further evaluation of the antibody effect in mammalian host models will be conducted in the future.

In summary, we validated scFv5 as an antibody that can antagonize SpuE function, downregulate the T3SS activity and attenuate the virulence of *P. aeruginosa*. Importantly, homologs that are virtually identical to SpuE (>99% identity) exist within the four prevalent multidrug resistant gram-negative bacteria designated as ESKAPE pathogens, namely *P. aeruginosa, A. baumannii*, *Enterobacter* and *K. pneumonia* (Supplementary Fig. 2). Thus, scFv5 represents a promising lead candidate

for the development of novel biologics for treatment of *P. aeruginosa* and it may serve as a template for the design of biologics for treatment of other ESKAPE pathogens.

Materials and Methods

Protein expression and purification

Apo-SpuE and SpuE-spermidine were expressed and purified as described previously [17] with a minor modification that protein was finally purified with a Superdex 200 26/600 column (GE Healthcare) preequilibrated in 20 mM HEPES, 100 mM NaCl, pH 7.5. Protein was concentrated to 10 mg/mL and stored in aliquots at −80 °C.

For expression of scFvs (VH-linker-VL-Flag tag), DNA encoding heavy and light variable domains was amplified by PCR using phagemid DNA as template. The DNA was cloned into pETDuet-2-3C-ss vector between BamHI and SalI restriction sites by following the infusion kit's instruction (Clontech, catalog no. 639648). pETDuet-2-3C-ss vector was engineered from pETDuet backbone vector (Novagen, catalog no. 71146-3) containing a 23-residue signal peptide (Sequence: MKKNIAFLLASMFVFSIATNAYA), a 6xHis tag and a 3C PreScission Protease cleavage site upstream of the gene. The constructs were verified by DNA sequencing and transformed into *E. coli* BL21 (DE3) that were grown at 37 °C in LB medium containing 100 μg/mL ampicillin. At OD600 of 0.6, protein expression was induced with 0.2 mM IPTG and cultures were grown overnight at 16 °C. Bacterial pellets were harvested by centrifugation, resuspended in 20 mM HEPES, 500 mM NaCl, pH 7.5, and lysed using a NANO homogenize machine (ATS Engineering Limited) at 1000 bar, 4 °C. After centrifugation, the supernatant was subjected to Talon resin affinity chromatography (Clontech) following manufacturer's instructions. After extensive washing, the target protein was eluted with 20 mM HEPES, 250 mM NaCl, 250 mM Imidazole, pH 7.5. After desalting into 20 mM HEPES, 100 mM NaCl, pH 7.5, His-tagged 3C protease (Takara, catalog no. 7360) was added and the sample was incubated overnight at 4 °C. The cleaved protein was separated from uncleaved protein and cleaved His-tag by a second Talon resin affinity chromatography. Protein was further purified with a Superdex 200 26/600 column (GE Healthcare), concentrated to 10 mg/mL in 20 mM HEPES, 100 mM NaCl, pH 7.5, and stored in aliquots at −80 °C.

Membrane penetrating peptide (MPP) was synthesized from Scipeptide Company (www.scipeptide.com). For expression of scFv5-MPP or control scFv-MPP (scFv-linker-MPP), the DNA was cloned into pETDuet-2-3C-ss-MPP vector between BamHI and HindIII restriction sites by following the infusion kit's instruction (Clontech, catalog no. 639648). pETDuet-2-3C-ss-MPP vector was engineered from pETDuet-2-3C-ss backbone vector by insertion of a DNA coding fragment for the linker-MPP using HindIII and NotI restriction sites. Strategy for expression and purification of scFv-MPP proteins was identical to that for scFv proteins.

Phage display selections

Phage display binding selections were performed as described [24] with a slight modification. In brief, a negative selection was first performed by incubation of library phage pool [24] with streptavidin-coated magnetic beads (Thermo Fisher Scientific, catalog no. 11206D). Biotinylated SpuE-spermidine was incubated with the phage pool and captured with streptavidin-coated magnetic beads. After washing, bound phage was eluted from the beads with 100 mM HCl and was amplified for subsequent rounds of selection by passage through *E. coli* XL1-blue. After three rounds of selection, 196 individual clones were assessed for binding to antigen by phage ELISA, as described [46]. Clones displaying at least 10-fold higher signal for binding to SpuE-spermidine compared with BSA were subjected to DNA sequencing to decode the sequences of the phage-displayed scFvs [47].

ELISAs

EC_{50} and IC_{50} values for purified scFvs binding to immobilized SpuE-spermidine were determined using direct binding ELISA or competitive ELISA, respectively, as described [48,49]. Simultaneous binding of antibodies to immobilized SpuE-spermidine was evaluated to map relative epitopes using methods similar to those described [49], by blocking immobilized SpuE-spermidine with saturating scFv protein and measuring subsequent binding of scFv-phage with horseradish peroxidase (HRP)-conjugated anti-M13 antibody (GE/Amersham/whatman, catalog no. 27-9421-01). ELISA binding curves were fit in GraphPad Prism (Version 8.1.0) using the log (agonist) versus response-variable slope model and the log (inhibitor) versus response-variable slope model from which EC_{50} and IC_{50} estimates were obtained, respectively.

P. aeruginosa genetic engineering

P. aeruginosa PAO1 was used as a parental strain for generation of the unmarked *spuE* deletion mutant. In brief, the DNA sequence of *spuE* encoding for amino acids 13–353 of SpuE was deleted by using the allelic exchange method, as described [16], except that pEX18Gm was used as the allelic exchange vector. Inactivation of the *spuE* gene in the PA14 strain was achieved by mutating the codon encoding for Trp34 of *spuE* (tgg) to a premature stop codon (taa) using the base editing system pnCasPA-BEC [50]. Inactivation of *spuE* was confirmed by sequencing.

P. aeruginosa and *E. coli* were grown in LB broth at 37 °C. Antibiotics were added when necessary as follows: for WT *P. aeruginosa*, 100 μg/mL spectinomycin (Spe); For Δ*spuE P. aeruginosa*, 100 μg/mL Spe, 100 μg/mL gentamicin (Gm); For *E. coli S17-1 λpir*, 20 μg/mL Gm.

0.7 mM spermidine was added to culture medium to induce T3SS expression, as described [16].

$$\text{LDH release} = (\text{OD}_{490} \text{ of sample} - \text{OD}_{490} \text{ of negative control}) / (\text{OD}_{490} \text{ of positive control} - \text{OD}_{490} \text{ of negative control})$$

$$\text{Cytotoxicity } (\%) = (\text{LDH release of sample} / \text{LDH release of WT } \textit{P. aeruginosa} \text{ PAO1 alone}) * 100$$

Western blot analysis

Western blot analysis was carried out according to standard protocols [51]. Briefly, overnight culture of *P. aeruginosa* PAO1 was inoculated and grown in fresh LB broth supplemented with appropriate scFv protein under T3SS-inducing conditions until log phase. Supernatant was collected and concentrated by fivefold in Amicon Ultra centrifugal filter tube (Merck/Millipore, catalog no. UFC900396) for detection of secreted ExoS. The primary and secondary antibodies used for ExoS blotting were antiexoenzyme S antibody (Abcam, catalog no. ab20031) and antichicken IgY antibody-HRP conjugate (Abcam, catalog no. ab6753), respectively.

RT-PCR analysis

P. aeruginosa was grown in LB broth containing appropriate scFv protein under T3SS-inducing condition until late log phase. Total RNA samples were extracted from fresh bacterial cultures using RNAprep kit (Tiangen biotech, cat no. DP430) and cDNA was synthesized by using TIANScript RT kit (Tiangen biotech, cat no. KR104) according to the manufacturer's instructions. Four selected T3SS genes (*exsC, popB, pscF*, and *pscQ*) were analyzed by RT-PCR as described [17]. 16S rRNA was used as a reference gene.

Cytotoxicity assay

Cytotoxicity assay was performed as described, with slight modification [52]. Briefly, overnight culture of *P. aeruginosa* was grown in LB broth under T3SS-inducing condition until log phase. The LB broth was supplemented with appropriate protein of three different concentrations dissolved in 1 × PBS (0.5 nM, 10 nM and 200 nM). 1×10^5 human bronchial epithelial A549 cells (ATCC CRM-CCL-185) in DMEM containing 10% fetal bovine serum (FBS) were seeded per well in 96-well cell culture plate (Corning, catalog no. 3599) and grown overnight. Bacteria were added to A549 cells at a multiplicity of infection (MOI) of 50 along with appropriate scFv protein of three different concentrations dissolved in 1 × PBS (0.5 nM, 10 nM, and 200 nM). The cultures were incubated for 2 h at 37 °C and 5% CO_2. Lactate dehydrogenase (LDH) activity released from lysed cells was determined by LDH cytotoxicity assay kit (Beyotime, catalog no. C0016). LDH release and cytotoxicity were calculated using the following equations:

The cytotoxicity of WT *P. aeruginosa* PAO1 alone was defined as 100%. The mean and the standard deviation (SD) were calculated from three independent experiments. Unpaired *t*-test with Welch's correction was performed for statistical analysis and P value less than 0.05 was considered to be a statistically significant difference.

C. elegans killing assay

Wild-type *C. elegans* N2 strains were obtained from the *Caenorhabditis* Genetics Center Database (CGC) and were maintained at 22 °C on NGM plates using *E. coli* OP50 as food (OP50/NGM). Washes and bleaching were performed according to the standard protocols [53].

P. aeruginosa killing experiments were performed as described [25], with some modifications. Briefly, *P. aeruginosa* were cultured overnight in LB medium supplemented with 0.7 mM spermidine (LB/spermidine medium), and 120 μL of overnight culture was transferred to 6 mL fresh LB/spermidine medium, supplemented with appropriate scFv protein. The cultures were grown at 37 °C with shaking at 200 rpm to log phase (OD_{600} ~1.0). The cultures were concentrated 10-fold to a final volume of 600 μL by centrifugation, mixed with 200 μL M9 buffer containing 70−110 synchronized wild type *C. elegans* adults, and transferred into 96-well plates. After incubation for 9−10 h at 25 °C, *C. elegans* were transferred to fresh OP50 plates and recovered for 5−6 h before being scored. As a positive control, the antibiotic Ciprofloxacin (Sigma-Aldrich) was used to treat *P. aeruginosa* infection at a final concentration of 50 μg/mL.

The mean and the standard deviation (SD) were calculated from three independent experiments. Unpaired *t*-test with Welch's correction was performed for statistical analysis after normalization of *P. aeruginosa* OD_{600} with regards to the corresponding survival rate in each group, and P value less than 0.05 was considered as statistically significant difference.

Isothermal titration calorimetry (ITC) analysis

ITC measurements were performed at 25 °C in a MicroCal ITC200 system (Malvern). Protein samples and spermidine were prepared in 20 mM HEPES, 100 mM NaCl, pH 7.5. Concentrations of proteins in the cell and

spermidine in the syringe were 20 or 200 μM, respectively. Assembly of apo-SpuE in complex with scFv5 follows the same procedure as that for SpuE-spermidine in complex with scFv5 for crystallization (see below). Spermidine was injected 20 times (1.0 μL for the first injection and 2 μL for other injections), with 120 s intervals between injections. The data were integrated in NITPIC and analyzed in SEDPHAT using global fits to a one-site binding model [54,55].

scFv5-SpuE protein complex purification and crystallization

Purified SpuE and scFv5 were mixed at 1:2 M ratio, incubated on ice for 1 h, and purified on a S200 26/600 column (GE Healthcare) preequilibrated in 20 mM HEPES, 100 mM NaCl, pH 7.5. Eluted complex was concentrated to 15 mg/mL for crystallization. Hanging-drop vapor diffusion method was used to grow crystals with 1 mL of reservoir solution. 1 μL of protein sample was mixed with 1 μL of 0.1 M Bis-Tris, 0.2 M Li_2SO_4, 25% polyethylene glycol 3350, pH 5.5. Before freezing into liquid nitrogen, crystals were transferred in serial steps to 0.1 M Bis-Tris, 0.2 M Li_2SO_4, 30% polyethylene glycol 3350, 20% glycerol, pH 5.5.

Data collection, structure determination and refinement

X-ray diffraction data from the crystals were collected at beamline BL19U (Shanghai Synchrotron Radiation Facility, China), and were scaled and merged with HKL-3000 [56]. The crystal of SpuE-spermidine-scFv5 complex belongs to space group $P2_1$. Molecular replacement was conducted using Phaser in Phenix [57]. The SpuE-spermidine search model was from PDB Code 3TTN with 100% sequence identity. The scFv5 search model without CDRs was generated in Swiss-Modeling [58] based on a scFv template (PDB code: 4BUH) with sequence identity of 52%. 18 copies of SpuE-spermidine and scFv5 were clearly identified within one ASU of SpuE-spermidine-scFv5 complex crystal.

Iterative model building in Coot [59] and refinement in Phenix Refine [57] were conducted to generate the final models of SpuE-spermidine in complex with scFv5. The stereochemical geometry of the models was checked using PROCHECK [60]. Structural figures were prepared using Pymol (www.pymol.org). Root mean square deviations (RMSD) were calculated in Dali server [32] and buried solvent accessible surface areas were calculated in PDBe PISA v1.52 [61]. Sequence alignments were conducted using CLUSTALW [62] and the figure was generated using Jalview [63]. The secondary structural elements of SpuE-spermidine were generated using DSSP [64] and shown above the sequences.

Molecular dynamics simulations

The X-ray structural coordinates of apo-SpuE (PDB code: 3TTL), SpuE-spermidine (PDB code: 3TTN) and SpuE-spermidine in complex with scFv5 (PDB code: 6KIM) were used as the input files and imported into the Maestro package of Schrodinger Suite v2019-1 (http://www.schrodinger.com/Maestro). All the structures were preprocessed using the Protein Preparation wizard [65] module with default settings. The PROPKA [66] module was used to predict the protonation states of all the residues at pH 7.0, and the hydrogen bonding network was subsequently optimized. Finally, the restrained minimization was performed using OPLS3e [67] force field for all the structures.

All the protein structures were processed with System Builder module and solvated into a cubic box by adding water molecules and 0.15 M NaCl. The proteins in the box had at least 10 Å buffering distance to the box boundary so that the interaction between its adjacent molecules and itself could be neglected. Subsequently, a few water molecules were replaced with Na^+ or Cl^- ions to keep the system in neutral state. Each system included approximately 51,000 and 94,000 atoms for the structures in the absence or presence of the antibody, respectively. Amber99SB-ILDN [68] force field with the TIP3P water model was used to describe interactions in proteins and solvent. The topology file and parameters of spermidine molecule were generated by AmberTools17 program [69] based on general Amber force field (GAFF) [70].

Molecular dynamic simulations were performed in the NPT ensemble at 310 K and 1 atm pressure using GPU-accelerated Desmond software [71]. The temperature and pressure were controlled using Nose-Hoover chain thermostat [72] and Martyna-Tobias-Klein barostat [73], respectively. The smooth particle mesh Ewald (PME) method was used for calculating the long range electrostatic interactions [74]. The independent simulations of 200 ns were performed for each of the three protein structures with coordinates saved every 0.1 ns for subsequent analysis. The mass center distance variation was analyzed using VMD script [75].

Accession numbers

Coordinates and structure factors have been deposited in the Protein Data Bank with accession number 6IKM.

Acknowledgements

Dr. Richard Lerner kindly provided the human scFv phage display library. Dr. Yawen He kindly provided pEX18Gm, *P. aeruginosa* PAO1 and *E. coli* S17-1 λpir. Dr. Huaying Zhao helped with ITC data analysis. We thank the staff of BL17B/BL18U1/BL19U1 beamlines at National Facility for Protein Science Shanghai (NFPS) and Shanghai Synchrotron Radiation Facility (SSRF), Shanghai, People's Republic of China, for assistance during data collection. This work was supported by the National

Natural Science Foundation of China (Grant No.: 31771006) to DHW.

Author Contributions

DHW initiated the project. DHW and SSS supervised the project. YZ performed experiments for characterization of EC_{50}, IC_{50}, epitope mapping, in vitro analysis of T3SS activity and attenuation of cytotoxicity towards A549. XDS performed phage library selections and crystallization of SpuE-spermidine in complex with scFv5. DHW solved and analyzed the crystal structure. YYQ and HHZ performed *C. elegans* experiments. HFY performed ITC experiments and protein purification. KS and FZ performed molecular dynamics simulation analysis. WZC and QJJ constructed the PA14 *SpuE* knockout. DHW and YZ wrote the manuscript. DHW, SSS and SM reviewed and edited manuscript.

Declarations of Interest

None.

Appendix A. Supplementary data

Supplementary data to this article can be found online at https://doi.org/10.1016/j.jmb.2019.10.026.

Received 27 July 2019;
Received in revised form 12 October 2019;
Accepted 20 October 2019
Available online 2 November 2019

Keywords:
multidrug resistant;
Pseudomonas aeruginosa;
type III secretion system;
SpuE;
antibody phage display;
spermidine importer

† Y.Z. and X.S. contributed equally to this work.

References

[1] J.N. Pendleton, S.P. Gorman, B.F. Gilmore, Clinical relevance of the ESKAPE pathogens, Expert Rev. Anti Infect. Ther. 11 (2013) 297–308.
[2] D.A. Rasko, V. Sperandio, Anti-virulence strategies to combat bacteria-mediated disease, Nat. Rev. Drug Discov. 9 (2010) 117–128.
[3] P. Keyser, M. Elofsson, S. Rosell, H. Wolf-Watz, Virulence blockers as alternatives to antibiotics: type III secretion inhibitors against Gram-negative bacteria, J. Intern. Med. 264 (2008) 17–29.
[4] M.J. Pallen, S.A. Beatson, C.M. Bailey, Bioinformatics, genomics and evolution of non-flagellar type-III secretion systems: a Darwinian perspective, FEMS Microbiol. Rev. 29 (2005) 201–229.
[5] A. Roy-Burman, R.H. Savel, S. Racine, B.L. Swanson, N.S. Revadigar, J. Fujimoto, et al., Type III protein secretion is associated with death in lower respiratory and systemic Pseudomonas aeruginosa infections, J. Infect. Dis. 183 (2001) 1767–1774.
[6] S.M. Rangel, M.H. Diaz, C.A. Knoten, A. Zhang, A.R. Hauser, The role of ExoS in dissemination of Pseudomonas aeruginosa during pneumonia, PLoS Pathog. 11 (2015), e1004945.
[7] J.L. Veesenmeyer, H. Howell, A.S. Halavaty, S. Ahrens, W.F. Anderson, A.R. Hauser, Role of the membrane localization domain of the Pseudomonas aeruginosa effector protein ExoU in cytotoxicity, Infect. Immun. 78 (2010) 3346–3357.
[8] A. Anantharajah, M.P. Mingeot-Leclercq, F. Van Bambeke, Targeting the type three secretion system in Pseudomonas aeruginosa, Trends Pharmacol. Sci. 37 (2016) 734–749.
[9] C. Van Delden, B.H. Iglewski, Cell-to-cell signaling and Pseudomonas aeruginosa infections, Emerg. Infect. Dis. 4 (1998) 551–560.
[10] T.L. Yahr, L.M. Mende-Mueller, M.B. Friese, D.W. Frank, Identification of type III secreted products of the Pseudomonas aeruginosa exoenzyme S regulon, J. Bacteriol. 179 (1997) 7165–7168.
[11] J.T. Barbieri, J. Sun, Pseudomonas aeruginosa ExoS and ExoT, Rev. Physiol. Biochem. Pharmacol. 152 (2004) 79–92.
[12] H. Sato, D.W. Frank, C.J. Hillard, J.B. Feix, R.R. Pankhaniya, K. Moriyama, et al., The mechanism of action of the Pseudomonas aeruginosa-encoded type III cytotoxin, ExoU, EMBO J. 22 (2003) 2959–2969.
[13] R. Balczon, N. Prasain, C. Ochoa, J. Prater, B. Zhu, M. Alexeyev, et al., Pseudomonas aeruginosa exotoxin Y-mediated tau hyperphosphorylation impairs microtubule assembly in pulmonary microvascular endothelial cells, PLoS One 8 (2013), e74343.
[14] T.C. Stevens, C.D. Ochoa, K.A. Morrow, M.J. Robson, N. Prasain, C. Zhou, et al., The Pseudomonas aeruginosa exoenzyme Y impairs endothelial cell proliferation and vascular repair following lung injury, Am. J. Physiol. Lung Cell Mol. Physiol. 306 (2014) L915–L924.
[15] T.L. Yahr, M.C. Wolfgang, Transcriptional regulation of the Pseudomonas aeruginosa type III secretion system, Mol. Microbiol. 62 (2006) 631–640.
[16] L. Zhou, J. Wang, L.H. Zhang, Modulation of bacterial Type III secretion system by a spermidine transporter dependent signaling pathway, PLoS One 2 (2007), e1291.
[17] D. Wu, S.C. Lim, Y. Dong, J. Wu, F. Tao, L. Zhou, et al., Structural basis of substrate binding specificity revealed by the crystal structures of polyamine receptors SpuD and SpuE from Pseudomonas aeruginosa, J. Mol. Biol. 416 (2012) 697–712.
[18] C.D. Lu, Y. Itoh, Y. Nakada, Y. Jiang, Functional analysis and regulation of the divergent spuABCDEFGH-spuI operons for polyamine uptake and utilization in Pseudomonas aeruginosa PAO1, J. Bacteriol. 184 (2002) 3765–3773.
[19] C. Wang, X. Liu, J. Wang, J. Zhou, Z. Cui, L.H. Zhang, Design and characterization of a polyamine derivative

inhibiting the expression of type III secretion system in Pseudomonas aeruginosa, Sci. Rep. 6 (2016) 30949.
[20] J. Wang, J. Wang, L.H. Zhang, Immunological blocking of spermidine-mediated host-pathogen communication provides effective control against Pseudomonas aeruginosa infection, Microb. Biotechnol. (2018).
[21] A.J. Michael, Polyamines in eukaryotes, bacteria, and archaea, J. Biol. Chem. 291 (2016) 14896–14903.
[22] A.E. Pegg, Functions of polyamines in mammals, J. Biol. Chem. 291 (2016) 14904–14912.
[23] A.O. Gevrekci, The roles of polyamines in microorganisms, World J. Microbiol. Biotechnol. 33 (2017) 204.
[24] H. Zhang, I.A. Wilson, R.A. Lerner, Selection of antibodies that regulate phenotype from intracellular combinatorial antibody libraries, Proc. Natl. Acad. Sci. U. S. A. 109 (2012) 15728–15733.
[25] Y. Briers, M. Walmagh, V. Van Puyenbroeck, A. Cornelissen, W. Cenens, A. Aertsen, et al., Engineered endolysin-based "Artilysins" to combat multidrug-resistant gram-negative pathogens, mBio 5 (2014) e01379-01314.
[26] E. Frithz-Lindsten, Y. Du, R. Rosqvist, A. Forsberg, Intracellular targeting of exoenzyme S of Pseudomonas aeruginosa via type III-dependent translocation induces phagocytosis resistance, cytotoxicity and disruption of actin microfilaments, Mol. Microbiol. 25 (1997) 1125–1139.
[27] M.W. Tan, S. Mahajan-Miklos, F.M. Ausubel, Killing of Caenorhabditis elegans by Pseudomonas aeruginosa used to model mammalian bacterial pathogenesis, Proc. Natl. Acad. Sci. U. S. A. 96 (1999) 715–720.
[28] K. Mathee, Forensic investigation into the origin of Pseudomonas aeruginosa PA14 - old but not lost, J. Med. Microbiol. 67 (2018) 1019–1021.
[29] T.W. Johnson, B. Bolanos, A. Brooun, R.A. Gallego, D. Gehlhaar, M. Jalaie, et al., Reviving B-factors: activating ALK mutations increase protein dynamics of the unphosphorylated kinase, ACS Med. Chem. Lett. 9 (2018) 872–877.
[30] A.K. Bronowska, Thermodynamics of ligand-protein interactions: implications for molecular design, in: J.C. Moreno-Pirajan (Ed.), Thermodynamics - Interaction Studies - Solids, Liquids and Gases, IntechOpen, Rijeka, 2011.
[31] J.A. Caro, K.W. Harpole, V. Kasinath, J. Lim, J. Granja, K.G. Valentine, et al., Entropy in molecular recognition by proteins, Proc. Natl. Acad. Sci. U. S. A. 114 (2017) 6563–6568.
[32] L. Holm, P. Rosenstrom, Dali server: conservation mapping in 3D, Nucleic Acids Res. 38 (2010) W545–W549.
[33] K. Hollenstein, D.C. Frei, K.P. Locher, Structure of an ABC transporter in complex with its binding protein, Nature 446 (2007) 213–216.
[34] C. Tang, C.D. Schwieters, G.M. Clore, Open-to-closed transition in apo maltose-binding protein observed by paramagnetic NMR, Nature 449 (2007) 1078–1082.
[35] F. Khalili-Araghi, J. Gumbart, P.C. Wen, M. Sotomayor, E. Tajkhorshid, K. Schulten, Molecular dynamics simulations of membrane channels and transporters, Curr. Opin. Struct. Biol. 19 (2009) 128–137.
[36] D.C. Rees, E. Johnson, O. Lewinson, ABC transporters: the power to change, Nat. Rev. Mol. Cell Biol. 10 (2009) 218–227.
[37] H.S. Garmory, R.W. Titball, ATP-binding cassette transporters are targets for the development of antibacterial vaccines and therapies, Infect. Immun. 72 (2004) 6757–6763.
[38] A.J. Rice, A. Park, H.W. Pinkett, Diversity in ABC transporters: type I, II and III importers, Crit. Rev. Biochem. Mol. Biol. 49 (2014) 426–437.
[39] S. Ahuja, L. Rouge, D.L. Swem, J. Sudhamsu, P. Wu, S.J. Russell, et al., Structural analysis of bacterial ABC transporter inhibition by an antibody fragment, Structure 23 (2015) 713–723.
[40] S.A. Mireku, M.M. Sauer, R. Glockshuber, K.P. Locher, Structural basis of nanobody-mediated blocking of BtuF, the cognate substrate-binding protein of the Escherichia coli vitamin B12 transporter BtuCD, Sci. Rep. 7 (2017) 14296.
[41] I. Zimmermann, P. Egloff, C.A. Hutter, F.M. Arnold, P. Stohler, N. Bocquet, et al., Synthetic single domain antibodies for the conformational trapping of membrane proteins, Elife 7 (2018).
[42] Y. Briers, R. Lavigne, Breaking barriers: expansion of the use of endolysins as novel antibacterials against Gram-negative bacteria, Future Microbiol. 10 (2015) 377–390.
[43] M. Thandar, R. Lood, B.Y. Winer, D.R. Deutsch, C.W. Euler, V.A. Fischetti, Novel engineered peptides of a phage lysin as effective antimicrobials against multidrug-resistant acinetobacter baumannii, Antimicrob. Agents Chemother. 60 (2016) 2671–2679.
[44] C.D. Sifri, J. Begun, F.M. Ausubel, The worm has turned–microbial virulence modeled in Caenorhabditis elegans, Trends Microbiol. 13 (2005) 119–127.
[45] N.D. Peterson, R. Pukkila-Worley, Caenorhabditis elegans in high-throughput screens for anti-infective compounds, Curr. Opin. Immunol. 54 (2018) 59–65.
[46] S. Birtalan, Y. Zhang, F.A. Fellouse, L. Shao, G. Schaefer, S.S. Sidhu, The intrinsic contributions of tyrosine, serine, glycine and arginine to the affinity and specificity of antibodies, J. Mol. Biol. 377 (2008) 1518–1528.
[47] M.P. Lefranc, C. Pommie, M. Ruiz, V. Giudicelli, E. Foulquier, L. Truong, et al., IMGT unique numbering for immunoglobulin and T cell receptor variable domains and Ig superfamily V-like domains, Dev. Comp. Immunol. 27 (2003) 55–77.
[48] S.S. Sidhu, B. Li, Y. Chen, F.A. Fellouse, C. Eigenbrot, G. Fuh, Phage-displayed antibody libraries of synthetic heavy chain complementarity determining regions, J. Mol. Biol. 338 (2004) 299–310.
[49] S. Miersch, B.V. Maruthachalam, C.R. Geyer, S.S. Sidhu, Structure-directed and tailored diversity synthetic antibody libraries yield novel anti-EGFR antagonists, ACS Chem. Biol. 12 (2017) 1381–1389.
[50] W. Chen, Y. Zhang, Y. Zhang, Y. Pi, T. Gu, L. Song, et al., CRISPR/Cas9-based genome editing in Pseudomonas aeruginosa and cytidine deaminase-mediated base editing in Pseudomonas species, iScience 6 (2018) 222–231.
[51] M. Eisenstein, Westward expansion, Nat. Methods 2 (2005) 796.
[52] P. Warrener, R. Varkey, J.C. Bonnell, A. DiGiandomenico, M. Camara, K. Cook, et al., A novel anti-PcrV antibody providing enhanced protection against Pseudomonas aeruginosa in multiple animal infection models, Antimicrob. Agents Chemother. 58 (2014) 4384–4391.
[53] T. Stiernagle, Maintenance of C. elegans, WormBook, 2006, pp. 1–11.
[54] H. Zhao, G. Piszczek, P. Schuck, SEDPHAT–a platform for global ITC analysis and global multi-method analysis of molecular interactions, Methods 76 (2015) 137–148.
[55] C.A. Brautigam, H. Zhao, C. Vargas, S. Keller, P. Schuck, Integration and global analysis of isothermal titration

calorimetry data for studying macromolecular interactions, Nat. Protoc. 11 (2016) 882–894.
[56] W. Minor, M. Cymborowski, Z. Otwinowski, M. Chruszcz, HKL-3000: the integration of data reduction and structure solution–from diffraction images to an initial model in minutes, Acta Crystallogr. D Biol. Crystallogr. 62 (2006) 859–866.
[57] P.D. Adams, P.V. Afonine, G. Bunkoczi, V.B. Chen, I.W. Davis, N. Echols, et al., PHENIX: a comprehensive Python-based system for macromolecular structure solution, Acta Crystallogr. D Biol. Crystallogr. 66 (2010) 213–221.
[58] M. Biasini, S. Bienert, A. Waterhouse, K. Arnold, G. Studer, T. Schmidt, et al., SWISS-MODEL: modelling protein tertiary and quaternary structure using evolutionary information, Nucleic Acids Res. 42 (2014) W252–W258.
[59] P. Emsley, K. Cowtan, Coot: model-building tools for molecular graphics, Acta Crystallogr. D Biol. Crystallogr. 60 (2004) 2126–2132.
[60] R.A. Laskowski, M.W. MacArthur, D.S. Moss, J.M. Thornton, PROCHECK: a program to check the stereochemical quality of protein structures, J. Appl. Crystallogr. 26 (1993) 283–291.
[61] E. Krissinel, K. Henrick, Inference of macromolecular assemblies from crystalline state, J. Mol. Biol. 372 (2007) 774–797.
[62] J.D. Thompson, D.G. Higgins, T.J. Gibson, W. CLUSTAL, Improving the sensitivity of progressive multiple sequence alignment through sequence weighting, position-specific gap penalties and weight matrix choice, Nucleic Acids Res. 22 (1994) 4673–4680.
[63] A.M. Waterhouse, J.B. Procter, D.M. Martin, M. Clamp, G.J. Barton, Jalview Version 2–a multiple sequence alignment editor and analysis workbench, Bioinformatics 25 (2009) 1189–1191.
[64] W. Kabsch, C. Sander, Dictionary of protein secondary structure: pattern recognition of hydrogen-bonded and geometrical features, Biopolymers 22 (1983) 2577–2637.
[65] G.M. Sastry, M. Adzhigirey, T. Day, R. Annabhimoju, W. Sherman, Protein and ligand preparation: parameters, protocols, and influence on virtual screening enrichments, J. Comput. Aided Mol. Des. 27 (2013) 221–234.
[66] M.H. Olsson, C.R. Sondergaard, M. Rostkowski, J.H. Jensen, PROPKA3: consistent treatment of internal and surface residues in empirical pKa predictions, J. Chem. Theory Comput. 7 (2011) 525–537.
[67] E. Harder, W. Damm, J. Maple, C. Wu, M. Reboul, J.Y. Xiang, et al., OPLS3: a force field providing broad coverage of drug-like small molecules and proteins, J. Chem. Theory Comput. 12 (2016) 281–296.
[68] K. Lindorff-Larsen, S. Piana, K. Palmo, P. Maragakis, J.L. Klepeis, R.O. Dror, et al., Improved side-chain torsion potentials for the Amber ff99SB protein force field, Proteins 78 (2010) 1950–1958.
[69] D.A. Case, I.Y. Ben-Shalom, S.R. Brozell, D.S. Cerutti, T.E. Cheatham III, V.W.D. Cruzeiro, et al., Amber 2018, University of California, San Francisco, 2018.
[70] J. Wang, R.M. Wolf, J.W. Caldwell, P.A. Kollman, D.A. Case, Development and testing of a general amber force field, J. Comput. Chem. 25 (2004) 1157–1174.
[71] K.J. Bowers, E. Chow, H. Xu, R.O. Dror, M.P. Eastwood, B.A. Gregersen, et al., Scalable algorithms for molecular dynamics simulations on commodity clusters, SC 2006 conference, Proceedings of the ACM/IEEE, 2006.
[72] G.J. Martyna, M.L. Klein, M.E. Tuckerman, Nosé-Hoover chains: the canonical ensemble via continuous dynamics, J. Chem. Phys. 97 (1992) 2635–2643.
[73] G.J. Martyna, D.J. Tobias, M.L. Klein, Constant pressure molecular dynamics algorithms, J. Chem. Phys. 101 (1994) 4177–4189.
[74] U. Essmann, L. Perera, M.L. Berkowitz, T. Darden, H. Lee, L.G. Pedersen, A smooth particle mesh Ewald method, J. Chem. Phys. 103 (1995) 8577–8593.
[75] W. Humphrey, A. Dalke, K. Schulten, VMD: visual molecular dynamics, J. Mol. Graph. 14 (1996) 33–38.